

1 **A dedicated robust instrument for water vapor generation at low-humidity for use with a laser water**  
2 **isotope analyzer in cold and dry polar regions.**

3  
4 Christophe Leroy-Dos Santos<sup>1</sup>, Mathieu Casado<sup>1,2</sup>, Frédéric Prié<sup>1</sup>, Olivier Jossoud<sup>1</sup>, Erik Kerstel<sup>3</sup>, Morgane  
5 Farradèche<sup>1</sup>, Samir Kassi<sup>3</sup>, Elise Fourré<sup>1</sup>, Amaëlle Landais<sup>1,\*</sup>

6  
7 <sup>1</sup> Laboratoire des Sciences du Climat et de l'Environnement, CEA-CNRS-UVSQ-Paris Saclay-IPSL, Gif-sur-  
8 Yvette, France

9 <sup>2</sup> Alfred Wegener Institut, Helmholtz Center for Polar and Marine Research, Potsdam, Germany

10 <sup>3</sup> Laboratoire Interdisciplinaire de Physique, CNRS - Université Grenoble Alpes, Grenoble, France

11 \* corresponding author: amaelle.landais@lsce.ipsl.fr

12

13 **Abstract**

14 Obtaining precise continuous measurements of water vapor isotopic composition in dry places (polar or  
15 high-altitude regions) is an important challenge. The current limitation is the strong influence of humidity  
16 on the measured water isotopic composition by laser spectroscopy instruments for low-humidity levels  
17 (below 3,000 ppmv). This problem is addressed by determining the relationships between humidity and  
18 measured  $\delta^{18}\text{O}$  and  $\delta\text{D}$  of known water standards. We present here the development of a robust field  
19 instrument able to generate water vapor, down to 70 ppmv, at very stable humidity levels (average  $1\sigma$   
20 lower than 10 ppmv). This instrument, operated by a Raspberry interface, can be coupled to a commercial  
21 laser spectroscopy instrument. It proved to be highly stable during autonomous operation over more than  
22 one year at the East Antarctic Concordia and Dumont d'Urville stations.

23

24

25 **1. Introduction**

26 The recent development of laser spectroscopy instruments now enables the continuous measurement of  
27 the isotopic composition of water vapor at many observation stations all around the world (Bailey et al.,  
28 2015; Bastrikov et al., 2014; Schmidt et al., 2010; Sodemann et al., 2017; Tremoy et al., 2011). In particular,  
29 the isotopic composition of the water vapor has proven to be a very useful tool to document moist synoptic  
30 events in many locations (Bonne et al., 2014; Guilpart et al., 2017). In polar regions, the water vapor  
31 isotopic signal is not only useful to detect the origin of moist air (Bréant et al., 2019; Kopec et al., 2014)  
32 but also to improve the interpretation of the isotopic composition of water in surface snow and ice core  
33 archives (Steen-Larsen et al., 2014). Indeed, exchanges are occurring after deposition between the surface  
34 snow and the water vapor leading to modifications of the isotopic composition of the former and hence  
35 of the archived ice (Casado et al., 2016, 2018; Ritter et al., 2016).

36 Obtaining continuous measurements of the water vapor isotopic composition at Concordia station in  
37 central Antarctica is a key scientific challenge since the deep ice core drilled there, EPICA Dome C, provides  
38 the oldest continuous water isotopic record to date (Jouzel et al., 2007). It is thus a key reference for the  
39 study of past climate, and a correct interpretation of the isotopic record relies on the quantification of the  
40 transfer function between climate parameters and water isotopic composition in ice, itself influenced by  
41 exchanges with water vapor in the upper layers of the firn (Casado et al., 2018). Such knowledge is also of  
42 uttermost importance for the interpretation of water isotope records from the starting deep drilling  
43 project “Beyond EPICA-Oldest Ice” (<https://www.beyondepica.eu>), whose aim is to drill a 1.5-million-year  
44 old ice core at the Little Dome C site located 40 km away from Concordia station, hence with similar low  
45 temperature and humidity conditions.

46 One of the main limitations of the current commercial instruments when deployed in polar regions is their  
47 relatively poor performance at low water vapor concentration. Generally, the precision of the measured  
48 isotopic ratios  $\delta^{18}\text{O}$  and  $\delta\text{D}$  rapidly worsens when the water mixing ratio decreases to humidity levels  
49 below 3,000-5,000 ppmv (part-per-million per volume) (Bonne et al., 2014; Weng et al., 2020). However,  
50 in remote continental areas in Greenland and Antarctica, temperatures in winter can drop to very low  
51 values, leading to humidity levels down to 10 ppmv (Genthon et al., 2017). Arguably one of the most  
52 extreme experiments for continuous measurement of the water vapor isotopic composition was the  
53 deployment of a commercial Picarro L2130-i instrument at the East Antarctic French-Italian station of  
54 Concordia where the mean annual temperature is around  $-54^{\circ}\text{C}$  and the humidity barely exceeds 1,000  
55 ppmv during the warmest summer days (Casado et al., 2016). For such applications, there are two major  
56 impacts of low-humidity on the raw isotopic signal: first, we generally observe an apparent increase in the  
57  $\delta^{18}\text{O}$  and  $\delta\text{D}$  with decreasing humidity level and second, the standard deviation associated with the  
58 continuous measurements of  $\delta^{18}\text{O}$  and  $\delta\text{D}$  of the water vapor increases. This can lead to overall  
59 uncertainties of several ‰ for  $\delta^{18}\text{O}$  and tens of ‰ for  $\delta\text{D}$ . It is thus of uttermost importance to have a  
60 correct determination of the humidity dependency of the water vapor isotopic ratios.

61 Commercial instruments from Picarro Inc. are usually associated with a Picarro Standard Delivery Module  
62 (SDM) designed to generate humidity at stable levels between 5,000 and 30,000 ppmv. Using such a set-  
63 up for humidity levels below 5,000 ppmv leads to large uncertainties in the determination of the humidity  
64 influence on the water vapor isotopic composition (e.g. Guilpart et al., 2017). These uncertainties are due  
65 both to the instability of the water vapor generation using the SDM (in terms of water concentration –  
66 humidity – and/or isotopic composition) and to the analytical noise in the spectroscopy measurements  
67 when the absorption signals are weak. An alternative commercial device is the LGR (Los Gatos Research)  
68 calibration system (Water Vapor Isotope Standard Source, WVISS), which uses a nebulizer to  
69 instantaneously evaporate micro-droplets of liquid water from a standard reservoir into a large (1 L)

70 vaporizing chamber (Dong and Baer, 2010). This system is very stable and well adapted for a humidity  
71 range between 2,500 and 25,000 ppmv (Aemisegger et al., 2012).

72 Several home-made water vapor injection systems have been developed with the specific aim to achieve  
73 a better stability of the generated humidity at low-humidity levels. A first approach is to use a dew point  
74 generator injecting small amounts of water into dry air (Lee et al., 2005; Wang et al., 2009). This approach  
75 is time consuming as it takes long to reach equilibrium and relies on a very precise knowledge of the  
76 temperature to quantify the isotopic fractionation. A method using a piezoelectric microdroplet generator  
77 into a dry air stream could generate water mixing ratios between 12 and 3,500 ppmv (Iannone et al., 2009;  
78 Sturm and Knohl, 2009; Sayres et al., 2009). However, adjustment of humidity level and long-term stability  
79 were difficult to obtain with such devices. Systems relying on the use of syringe pumps were also built by  
80 Gkinis et al. (2010) and Tremoy et al. (2011): a small fraction of the input stream of liquid water is  
81 introduced into a hot oven where water is vaporized in the presence of a dry air flow. These systems cover  
82 humidity range between 2,000 and 30,000 ppmv. Finally, bubbler systems, in which dry air flows through  
83 a large volume of water to create saturated vapor, are very robust but can only produce water vapor at  
84 high-humidity levels (Ellehoj et al., 2013). The aforementioned devices are unfortunately not well suited  
85 for automatic long-term operation at low-humidity levels. During the 2014-2015 summer field season at  
86 Concordia station in Antarctica, a home-made humidity generator specifically designed for low-humidity  
87 levels (Landsberg, 2014) has been deployed (Casado et al., 2016). The device used dual high-precision,  
88 low-volume, syringe pumps to generate stable humidity levels at two different isotopic compositions over  
89 the range from 100 to 800 ppmv (Casado et al., 2016). Unfortunately, we observed quite a large scattering  
90 among the isotopic values measured at similar humidity levels, as well as a large discrepancy between the  
91 humidity dependency of the water isotopic ratios measured in the field and the one measured in the  
92 laboratory. Upon return to the laboratory, these defaults were traced primarily to tiny leaks in the water  
93 supply lines to the syringes.

94 Therefore, we re-engineered the prototype by Landsberg (2014) in order to develop a robust and  
95 autonomous device for stable low-level humidity generation for the purpose of precise humidity  
96 calibration of spectroscopic instruments. Such devices have now been operating with minimum manual  
97 intervention for more than one year at two polar stations in Antarctica, Dumont d'Urville and Concordia,  
98 coupled to Picarro laser spectroscopy instruments. We detail here the technical description of the  
99 instrument and show key performance characteristics, enabling, for instance, a discussion of small  
100 amplitude signals such as the diurnal variability of the water vapor isotopic composition in remote dry  
101 sites in East Antarctica.

102

103 **2. New vapor generator for low-humidity levels**

104

105 The low-humidity level generator (LHLG) developed here relies on the same principle as the one developed  
 106 by Landsberg (2014), i.e., a steady, undersaturated evaporation of a liquid water droplet at the tip of a  
 107 needle into a dry air stream inside a small evaporation chamber. Based on this first prototype, the  
 108 instrument has been remodeled including a specific hardware and software design.

109

## 110 2-1-Physical principle

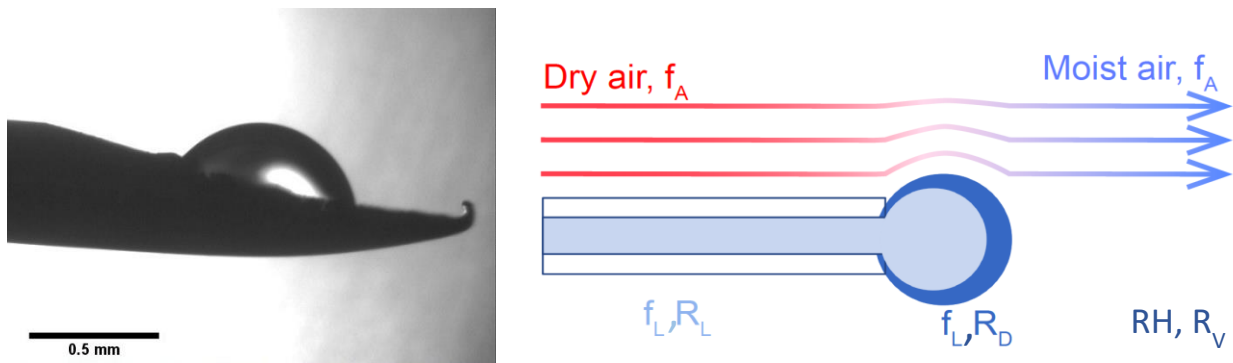
111 The LHLG is based on undersaturated evaporation of a small droplet at the tip of a needle (Figure 1). Liquid  
 112 water is pushed through a needle around which dry air is flowing. Dry air is obtained from a bottle of high  
 113 purity synthetic air with pressure regulation through two manometers connected in series. The mass flux  
 114 of water  $f_L$  is kept low compared to the air mass flow  $f_A$  so that the relative humidity  $RH$  of the downstream  
 115 moist air flow remains low ( $RH < 0.1$ ). Therefore, the air stays largely undersaturated and its humidity is  
 116 controlled only by the flow of liquid water in the needle and that of the dry air upstream of it. The mixing  
 117 ratio (or humidity) of the air as classically provided by a Picarro instrument is given by:

118

$$119 \quad MR = \frac{d_{H_2O} \times f_L \times R \times T_{st}}{f_A \times P_{st} \times M_{H_2O}} \quad (\text{eq. 1})$$

120

121 where  $d_{H_2O} = 1000 \text{ kg m}^{-3}$  is the density of water,  $R = 8.314 \text{ J mol}^{-1} \text{ K}^{-1}$  is the universal gas constant,  $T_{st} =$   
 122  $293.15 \text{ K}$  and  $P_{st} = 1013.25 \text{ hPa}$  are standard conditions of temperature and pressure and  $M_{H_2O} = 18.10^{-3}$   
 123  $\text{kg mol}^{-1}$ .



124

125 **Figure 1:** Evaporation of a droplet in the humidity generator chamber: left, picture from the prototype from  
 126 Landsberg (2014); right, schematics of the water molecules being transferred to the air flow (Casado,  
 127 2016).

128

129 Physically, when the flux of water or air is changed, there is first a transient regime during which the radius  
 130 of the droplet changes, modifying the evaporative surface and therefore the humidity of the outgoing air.  
 131 Once a stationary regime is reached, the radius of the droplet is stabilized and the humidity is given by

132 equation 1. In this regime, there is no accumulation of water molecules in the system and therefore the  
133 isotopic composition of the vapor produced is equal to the isotopic composition of the liquid water  
134 injected in the needle:  $R_V = R_L$  (note that because of the fractionation during the transition phase, the  
135 isotopic composition of the droplet  $R_D$  is different from  $R_L$  and  $R_V$ , see Kerstel, 2020). When changing the  
136 flux of evaporating water, we modify the size of the evaporating surface and therefore the radius of the  
137 drop. The evolution of the radius of the drop can be obtained from the resolution of a non-linear  
138 differential equation of the volume  $V$  of the drop:

139

$$140 \quad dV/dt = f_L - f_{evap} \quad (\text{eq. 2})$$

141

142 where  $f_{evap} = k_e \times S$  is the evaporation flux depending of  $k_e$ , the evaporation rate, and  $S$ , the surface area of  
143 the drop exposed to the dry air. A good approximation is to consider the shape of the drop as a fraction of  
144 a sphere of variable radius intercepted by the surface of a disk of constant radius (the syringe tip). By  
145 solving numerically the differential equation (2), it is possible to faithfully simulate the behavior of the  
146 device under changing conditions (Kerstel, 2020). This numerical approach validates the theoretical  
147 explanation of the undersaturated evaporation of the droplet. Importantly, it is noted that in steady-state  
148 as is the case for our application, the isotopic composition of the generated humid air is identical to that  
149 of the injected water stream, and therefore does not depend on the infusion rate, nor on the specific  
150 humidity.

151

## 152 **2-2- Instrument conception**

153

### 154 - **Technical realization**

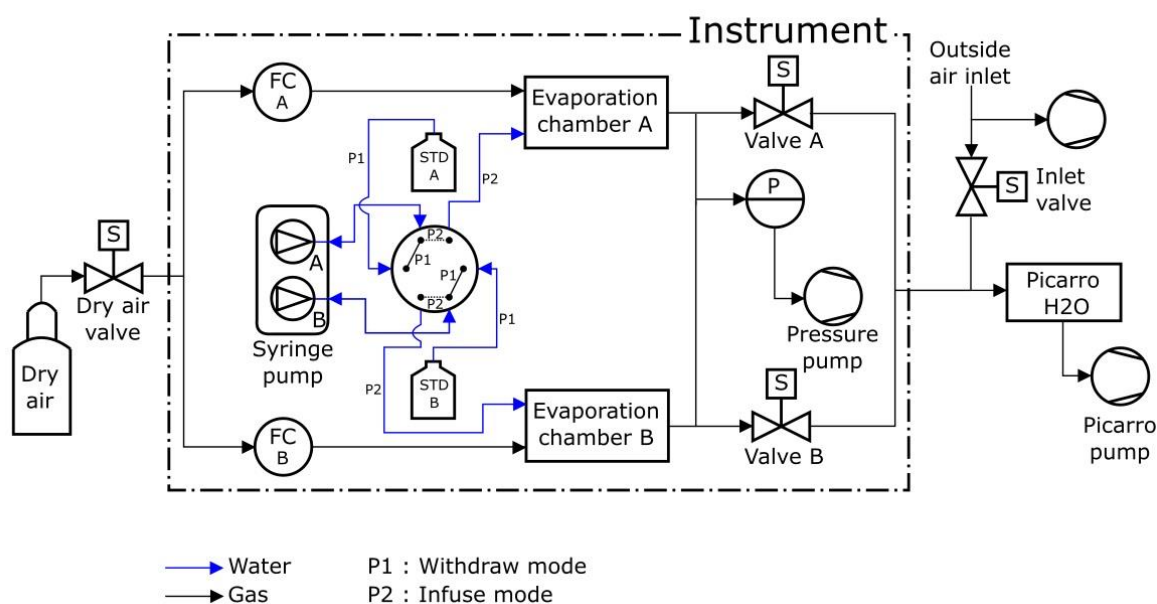
155 As the LHLG relies on operating in a stationary regime, it is important that the dry air input and the water  
156 input are steady. Thus, the air and water fluxes, as well as the air pressure in the evaporation chamber are  
157 controlled by electronic PID regulators. Temperature intervenes through its effect on fractionation and  
158 the evaporation rate (apart from a negligible effect on the flow controller stability), which could lead to a  
159 departure from steady-state operation. For these reasons, the temperature of the evaporation chambers  
160 was maintained at 20°C (within 1°C over 24 hours).

161 The dry air flux is regulated by a high-precision mass flow controller (Vögtlin GSC-A9TS-DD22), that has an  
162 operating range from 6 to 600 sccm ( $\text{std cm}^3 \text{ min}^{-1}$ ) and an accuracy of 3.3 sccm. The water flux is regulated  
163 by a high-precision syringe pump (Harvard Apparatus Pump 11 Pico Plus Elite Dual), which can produce a  
164 water flow down to  $10.8 \text{ pL min}^{-1}$  with an accuracy of 0.35 % using syringes with a volume ranging from  
165  $10 \text{ }\mu\text{L}$  to  $250 \text{ }\mu\text{L}$ . We operate in the routine mode with a dry air flow of 300 sccm and a water flow between  
166  $0.02$  to  $0.5 \text{ }\mu\text{L min}^{-1}$  using mainly 50 or 100  $\mu\text{L}$  syringes. A syringe pump is equipped with two syringes that

167 provide two water flows into two evaporation chambers in parallel (Figure 2). Each syringe is connected  
 168 to a water reservoir and to an evaporation chamber by a double 3-way liquid valve (Rheodyne MXX777603)  
 169 switching from an “infuse” mode to a “withdraw” mode to refill the syringes. The water in the water  
 170 reservoirs is sampled every month to check its isotopic composition and renewed when the level of water  
 171 is below half the maximum level. A maximum evolution of the isotopic composition of the lab-standard  
 172 filling the water reservoirs has been observed as 0.05‰ and 0.5‰ respectively for  $\delta^{18}\text{O}$  and  $\delta\text{D}$  over a 2-  
 173 month period.

174 A major change to the instrument designed by Landsberg (2014) is the introduction of the double 3-way  
 175 valve with leak-tight connections and an internal volume of 1.9  $\mu\text{L}$ . This modification is an important  
 176 improvement as it enables automatic handling of the lab-standards from a reservoir to the evaporation  
 177 chamber with a robust connection, avoiding in particular potential air bubbles in the water flow. Indeed,  
 178 the compressibility of air bubbles trapped in the water flow can lead to flow irregularities by amplification  
 179 of small non-linearities in the progression of the syringe plunger. This would lead to non-steady state  
 180 operation, which in turn would create artefacts in the humidity and isotopic composition, reducing the  
 181 performance of the calibration device (see Kerstel 2020). In addition, the 3-way valve provides the  
 182 opportunity of a "withdrawn" mode in which the syringes draw lab-standard water from a reservoir. When  
 183 equipped with 100- $\mu\text{L}$  syringes, the instrument can operate for several hours up to one day between refills.  
 184 With the addition of the auto-refill option and the effective suppression of bubbles, the instrument can be  
 185 used unattended for many months, as required for an Antarctic winter field campaign.

186



190  
191 The evaporation chambers are stainless steel cylinders equipped with specific connectors (Swagelok Ultra-  
192 Torr SS-4CD-TW-25) holding silicon rubber septa through which needles are inserted toward the middle of  
193 the chamber. The pressure in both chambers is regulated by a pressure controller (Bronkhorst P-702CV-  
194 1K1A-AAD-22-V) with a precision of 3 mbar in a range from 0 to 1,000 mbar. This pressurization of the two  
195 chambers combined with the relatively high flow (higher than required by the infrared spectrometers)  
196 enables maintaining a steady state whether or not the infrared spectrometer is connected, and increases  
197 the time efficiency of calibration procedures. The spectrometer is not sensitive to the inlet pressure, the  
198 precision of the pressure controller is not an essential aspect. On the contrary, the precision of the flow  
199 controller is key for the precision of the humidity level produced by the instrument: it is of 1% for the air  
200 flow which is comparable to the precision of the measurement of the humidity level with the optical  
201 spectrometer. When the instrument is connected to the infrared spectrometer, the excess humid air flow  
202 is exhausted to the room through the pressure pump and the spectrometer only pumps what is required  
203 (Figure 2).

204 The control of the instrument is ensured by a Raspberry Pi that can be interfaced to a Picarro water  
205 analyzer (L2130-i in our case) in sequencer mode (see below). The hardware has been designed to meet  
206 the specifications dictated by field conditions: 1) All components are fixed in a transportable case (except  
207 the dry air bottle), isolated from vibration by an anti-vibration foam. 2) A panel of connectors (HDMI, USB,  
208 Ethernet, etc.) ensures the accessibility to the instrument when it is closed. 3) The electrical and electronic  
209 parts (e.g. power supply, Raspberry Pi) are separated from the rest of the instrument (e.g. sensors, gauges).  
210 Both the electrical and electronic parts are fully and easily accessible in case of failure.

211

#### 212 - **Software details**

213 The control software has been developed using open source Python libraries and homemade drivers,  
214 including a user interface displaying the state of relevant components and the value of the different  
215 sensors. The software (HumGen) can be downloaded on line (<https://github.com/ojsd/humgen>;  
216 <https://doi.org/10.5281/zenodo.4003465>).

217 The LHLG can operate in eight different states, each state representing a specific setup for each element  
218 (valves position, syringe pump infusion rate, dry air flow rate, pressure). Those eight states can be divided  
219 into three categories: a routine mode, an expert mode and a humidity dependence calibration mode. The  
220 simple mode is composed of six predefined states referring to the classic isotopic calibration in everyday  
221 routine operation (Table 1): 1) measurement of the outside air water vapor isotopic composition; 2) drying  
222 of the cavities; 3) "humidity boost", in order to reach faster the desired humidity level in the cavities; 4)  
223 injection of the standard A in the corresponding evaporation chamber at a set humidity level; 5) injection  
224 of the standard B in the corresponding evaporation chamber; 6) refill of the syringes. The expert mode is

225 useful to adjust each parameter manually: flow rates on the controllers FCA and FCB, opening of the  
 226 electrovalves A and B, mode (infuse or withdraw) and infused rate for the syringe pump, pressure  
 227 regulation, state of the double three-way valve, activation of the pressure pump at the exhaust, opening  
 228 of external electrovalves from the dry air tank and to the inlet (Figure 2). The humidity dependence  
 229 calibration mode produces a scale of increasing humidity steps in the evaporation chambers (e.g. from 100  
 230 ppmv to 1000 ppmv, through steps of 100 ppmv for 50 minutes for each standard). The details of the  
 231 sequence (standard type, humidity level and duration of each step) is defined in a text file by the operator  
 232 from the Raspberry interface, the Raspberry being itself connected to Ethernet for remote access.

233 The Picarro L2130-i analyser has an External Valve Sequencer, which is able to turn on/off up to six  
 234 electrovalves and create loop sequences with defined durations for each step of the sequence. This tool  
 235 can be diverted from its original purpose by using it as a 6-digit code: each of the humidity generator state  
 236 is associated with a code. When the Picarro Valve Sequencer matches one of the state code, this state is  
 237 triggered on the humidity generator. This eases both the operator's activities and the data post-treatment,  
 238 because the current valve status - thus the calibration instrument state - is saved in the analyzer output  
 239 data file, in the "ValveMask" column. The Raspberry inside the LHLG reads the Valve Sequencer state code  
 240 using the Picarro's Remote Control Interface (a RS232 serial connection through one of the rear-face DB9  
 241 connector).

242

States (min)	Flow FCA (sccm)	Flow FCB (sccm)	Valve A	Valve B	Syringe Pump ( $\mu$ L/min)	Inlet Valve	Dry air Valve	Pressure controller (mbar)	Pressure Pump for exhaust	Double 3-way valve
Outside air (1100)	0	0	Closed	Closed	0	Open	Closed	Off	Off	To chamber
Drying (20)	400	400	Open	Open	0	Closed	Open	Off	Off	To chamber
Boost (0.7)	300	300	Open	Open	Infuse at 2.5	Closed	Open	905	On	To chamber
Standard A (50)	300	150	Open	Closed	Infuse at 0.25	Closed	Open	905	On	To chamber
Standard B (50)	150	300	Closed	Open	Infuse at 0.25	Closed	Open	905	On	To chamber



Reset (1)	Closed	Closed	Closed	Closed	Withdraw max speed	Open	Closed	Off	Off	From standard
--------------	--------	--------	--------	--------	-----------------------	------	--------	-----	-----	------------------

243 **Table 1:** Typical routine sequence of measurements + calibration for two standards A and B at 1000 ppmv  
244 for a measurement site located at sea level. No mixing occurs between standards A and B during steps  
245 “Standard A” and “Standard B” (see supplementary text S1).

246 Note that the humidity dependence mode and the expert mode can also be included in the valve sequencer  
247 but are not used in a daily calibration routine.

248  
249 A set of tools has been developed to quickly check daily calibration. In the field, analyzer and LHLG data  
250 are archived daily and sent to the laboratory, i.e. at LSCE, Gif sur Yvette. They are checked semi-  
251 automatically once a week to warn maintenance personnel in the event of a malfunction.

252  
253 **3- Performance of the instrument**  
254 While the stability of the instrument has been tested over a large range of parameters (supplementary  
255 Table S2), air flow and infusion rate have been adjusted to optimize the stability of the generated vapor  
256 while minimizing the dry air consumption. The LHLG is able to generate stable levels of humidity (drift  
257 lower than 20 ppmv over one hour and  $1\sigma$  below 10 ppmv over 10 minutes) from 70 ppmv to 2,400 ppmv  
258 following the optimal set-points shown in Table 2.

Humidity (ppmv)	Infusion rate ( $\mu\text{L}/\text{min}$ )	Dry Air flow (sccm)
80	0.01	300
160	0.02	300
320	0.04	300
800	0.1	300
1200	0.15	300
1600	0.2	300
2400	0.3	300

260  
261 **Table 2:** Set-points for water infusion rate and dry air flow at a temperature of 20°C.  
262

263 **3-1- No fractionation during water vaporization in the cavity**

264 We have checked that there was no fractionation of the water during its transfer from the bottles to the  
265 syringe pump, then from the syringe to the moist air generated in the vaporization chamber through the  
266 following tests.

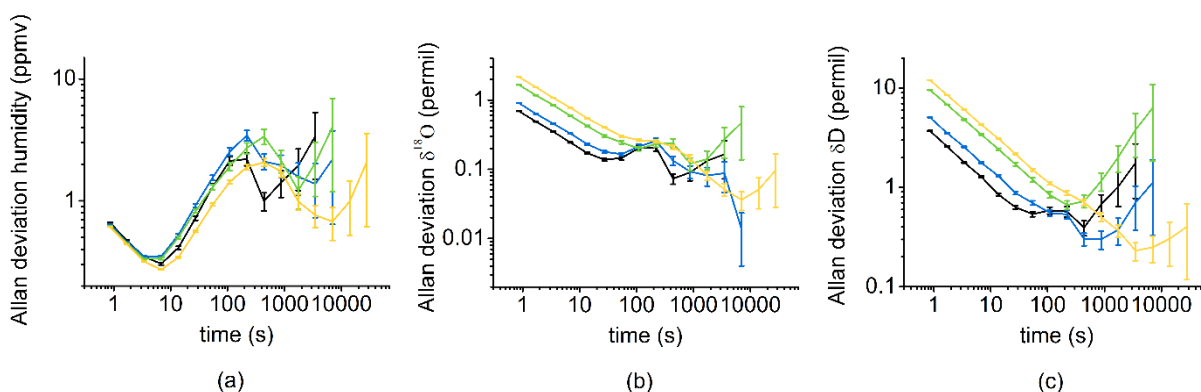
267 First, the isotopic composition of three different lab-standards calibrated against VSMOW at LSCE (H<sub>2</sub>O-  
268 CO<sub>2</sub> equilibration followed by IRMS for  $\delta^{18}\text{O}$ ; Cavity RingDown Spectroscopy for  $\delta\text{D}$ ; calibrated every 3  
269 years using VSMOW and VSLAP provided by IAEA) have been compared, after their generation by the

270 present LHLG and by the commercial SDM, both at a humidity of 2,000 ppmv over 50-min time spans. The  
 271 measured  $\delta^{18}\text{O}$  and  $\delta\text{D}$  values agreed to within 0.5‰ and 2‰, respectively, for the 3 lab-standard waters  
 272 calibrated against VSMOW: EPB ( $\delta^{18}\text{O} = -6.24$  ‰;  $\delta\text{D} = -43.6$  ‰), NEEM ( $\delta^{18}\text{O} = -33.50$  ‰;  $\delta\text{D} = -257.2$  ‰),  
 273 FP5 ( $\delta^{18}\text{O} = -48.33$  ‰;  $\delta\text{D} = -383.5$  ‰). Second, the measured isotopic composition of the same standard  
 274 (FP5) generated at different humidity levels between 1,000 and 2,400 ppmv by the SDM and the LHLG  
 275 show the same  $\delta^{18}\text{O}$  ( $\delta\text{D}$ ) evolution with humidity within respective uncertainties (Supplementary Figure  
 276 S1).

277

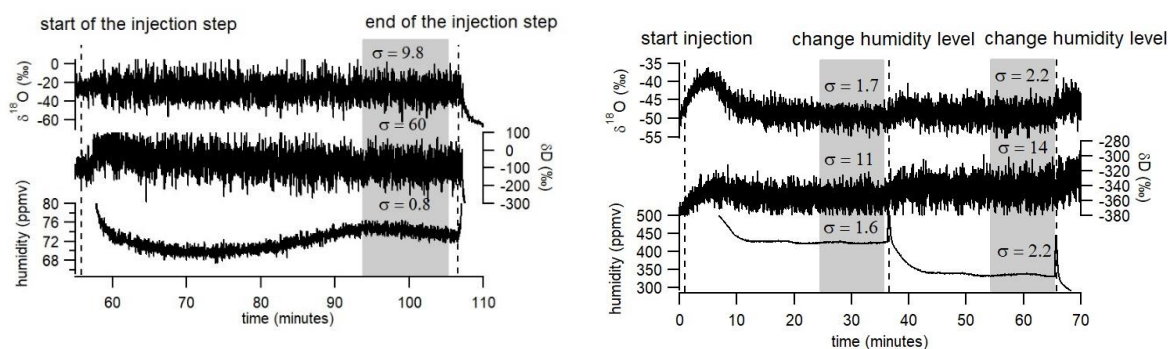
### 278 3-2- Stability of the water vapor delivery

279



280

281 **Figure 3:** Allan variance over 4 hours for different humidity levels (black 1,080 ppmv; blue 770 ppmv; green  
 282 400 ppmv; yellow 320 ppmv) for humidity (a),  $\delta^{18}\text{O}$  (b) and  $\delta\text{D}$  (c).



283 **Figure 4:** Records of  $\delta^{18}\text{O}$ ,  $\delta\text{D}$  and humidity over 3 humidity plateaus (72 ppmv on the left, 425 and 335  
 284 ppmv on the right) obtained with the LHLG. The grey rectangles indicate the period (10 min) over which the  
 285 average values are kept for calibrating the data generated by a L2130-i analyzer.

286

287

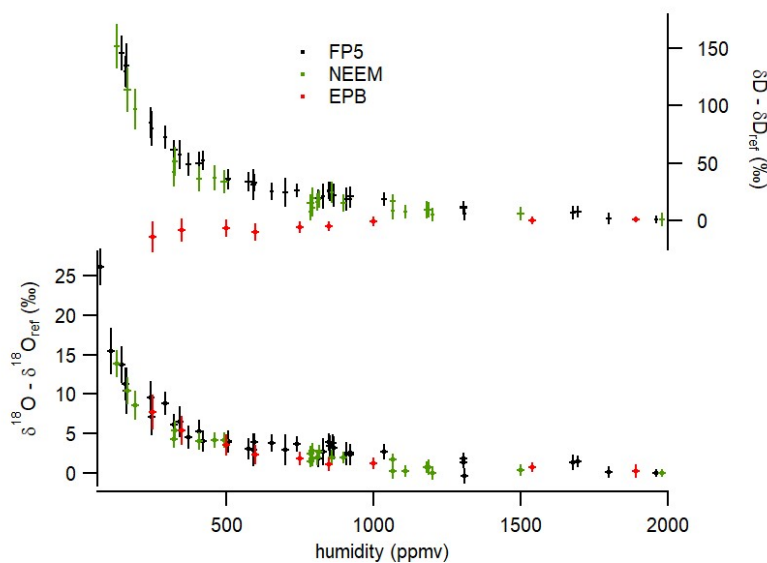
288 Figure 3 displays the Allan variance in  $\delta^{18}\text{O}$ ,  $\delta\text{D}$  and humidity over 4 hours for different humidity levels. The  
 289 humidity variance always stays below 10 ppmv over the 4 hours test and the  $\delta^{18}\text{O}$  /  $\delta\text{D}$  Allan variances

290 display minimum values below 0.1 ‰ and 0.8 ‰ respectively (the Allan variance of  $\delta^{18}\text{O}$  and  $\delta\text{D}$  are  
 291 however strongly dependent on the analyzer and on the humidity level). In the routine mode (Figure 4),  
 292 we perform plateaus of 30 to 50 minutes (50 minutes when the instrument is unattended since the time  
 293 to reach the plateau varies between a few minutes to 30 minutes). We then select the last 10 minutes  
 294 before the following switch of the instrument to measure the average level of humidity and the isotopic  
 295 ratios,  $\delta^{18}\text{O}$  and  $\delta\text{D}$ . We also calculate the associated standard deviations and reject the values if the  
 296 humidity standard deviation exceeds 30 ppmv over these last 10 minutes. In Figure 4, one observes that  
 297 the standard deviations for humidities generated in the routine mode are actually much lower. The  
 298 corresponding standard deviations for the isotopic ratios ( $\delta^{18}\text{O}$  and  $\delta\text{D}$ , see values indicated in Figure 4)  
 299 increase with decreasing humidity, reflecting the decrease of the molecular absorption signal recorded by  
 300 the L2130-i laser analyzers. This has an obvious impact on the determination of the relationship between  
 301 humidity and water vapor isotopic composition.

302 The performance of the present LHLG can be compared to the performance of the SDM (see  
 303 Supplementary Figures S1 and S2). First (Figure S2), a comparison has been performed at a humidity level  
 304 of 800 ppmv, for which we have numerous daily calibrations performed with a SDM from a 4.5 years field  
 305 deployment in Svalbard (Leroy-Dos Santos et al., 2020). The best SDM performance displays a standard  
 306 deviation  $1\sigma$  of 31 ppmv, which is significantly worse than the performance of the LHLG (standard  
 307 deviation  $1\sigma$  lower than 10 ppmv on average and down to 2 ppmv for 30% of the generated humidity  
 308 plateaus). Second (Figure S1), while we measure the same influence of humidity on measured  $\delta^{18}\text{O}$  and  $\delta\text{D}$   
 309 either with the SDM or with the LHLG, the  $1\sigma$  values on humidity levels are much larger for the SDM than  
 310 for the LHLG.

311

### 312 3-3- Determination of the influence of humidity on water vapor isotopic composition



313

314 **Figure 5:** Influence of humidity on the isotopic composition ( $\delta^{18}\text{O}$  and  $\delta\text{D}$ ) of the vapor obtained with the  
315 LHLG with 3 water lab-standards. The error bars are calculated as the standard deviation ( $1\sigma$ ) over the  
316 generated values by the L2130-i instrument during 10 minutes at 1 second resolution (i.e. without any pre-  
317 averaging of the raw dataseries). The  $\delta^{18}\text{O}_{\text{ref}}$  and  $\delta\text{D}_{\text{ref}}$  are the values of the injected water standards at  
318 2,000 ppmv.

319  
320 Contrary to the commercial SDM, which hardly produces stable and reproducible humidity levels below  
321 500 ppmv, the LHLG was able to daily produce stable 10-minute humidity plateaus over the range from 70  
322 ppmv to 2,400 ppmv with an associated standard deviation of the order of 10 ppmv over more than one  
323 year at the Concordia and Dumont d'Urville stations (installation in December 2018). The stability of the  
324 LHLG allows a robust quantification of the L2130-i analyzer drift thanks to a daily measurement of the  
325 same water isotopic standard reference (see Table S3 showing actually no measurable drift over a 3-week  
326 period). It also permits the characterization of the measurement non-linearities observed at low-humidity  
327 (Figure 5). The more than one-year long Concordia and Dumont d'Urville datasets showed that the  
328 humidity dependence of  $\delta^{18}\text{O}$  and  $\delta\text{D}$  did not vary measurably. The uncertainty of the obtained calibration  
329 curve can be attributed entirely to the L2130-i  $\delta^{18}\text{O}$  and  $\delta\text{D}$  measurements. In other words, the uncertainty  
330 bars in the horizontal (x-) axis in Figure 5, associated with the LHLG, are negligible.

331 Our data show a result already observed in Weng et al. (2020): while the dependency of  $\delta^{18}\text{O}$  and  $\delta\text{D}$  to  
332 humidity is similar for low  $\delta^{18}\text{O}$  and  $\delta\text{D}$  lab-standards (NEEM and FP5), we observe a different behavior for  
333 the  $\delta\text{D}$  vs humidity relationship for the high  $\delta^{18}\text{O}$  and  $\delta\text{D}$  lab-standard EPB. This result strengthens the  
334 recommendation of Weng et al. (2020) to use two water standards in the range of the measured water  
335 vapor isotopic composition to best calibrate our final data. In our case, our applications were in Antarctica,  
336 so that we used our two lowest lab-standards (NEEM and FP5). For the two standards and for this particular  
337 Picarro L2130-i (results are expected to depend on the instrument), the same dependency of isotopic  
338 composition vs humidity is observed. We express this dependency as the relationship between the  
339 difference in  $\delta\text{D}$  or  $\delta^{18}\text{O}$  between the measured value at the given humidity and the value of the same  
340 standard measured at a humidity of 2,000 ppmv. The experimental data for NEEM and FP5 from Figure 5  
341 are fitted through polynomial functions with respect to humidity  $h$  (in ppmv):

342  
343 
$$\delta^{18}\text{O} - \delta^{18}\text{O}_{\text{ref}} = 3.97 \times 10^{-18} \times h^6 - 3.59 \times 10^{-14} \times h^5 + 1.28 \times 10^{-10} \times h^4 - 2.31 \times 10^{-7} \times h^3 + 2.19 \times 10^{-4} \times h^2 - 1.06 \times 10^{-1} \times h +$$
  
344 23.7 (eq. 3)

345 
$$\delta\text{D} - \delta\text{D}_{\text{ref}} = 6.86 \times 10^{-17} \times h^6 - 6.00 \times 10^{-13} \times h^5 + 2.08 \times 10^{-9} \times h^4 - 3.61 \times 10^{-6} \times h^3 + 3.31 \times 10^{-3} \times h^2 - 1.54 \times h + 313$$
 (eq.  
346 4)

347

348 After this correction, the measured values corrected from humidity dependence are corrected using the  
349 comparison of the measured values of the 2 standards at 2,000 ppmv to their VSMOW calibrated values  
350 as explained in section 3.5 below.

351

### 352 **3.5- Accuracy of the system**

353 The accuracy of the system has been addressed performing a 2-standard calibration and measuring a third  
354 standard treated as an unknown. We used two lab-standards calibrated vs VSMOW with large  $\delta^{18}\text{O}$  and  
355  $\delta\text{D}$  differences (EPB and FP5) and used the lab-standard NEEM, also independently calibrated against  
356 VSMOW. The 3 lab-standards have been vaporized at 800 ppmv and measured by the same L2130-i  
357 analyzer.

358

Standard	VSMOW calibrated value	Measured value at 800 ppmv	Measured value corrected from humidity dependence (Equation 1)
EPB	-6.24 ‰	-8.27 ‰	-10.78 ‰
NEEM	-33.5 ‰	-34.48 ‰	-36.99 ‰
FP5	-48.33 ‰	-49.02 ‰	-51.53 ‰

359

360 **Table 3:** Comparison of measured vs VSMOW calibrated  $\delta^{18}\text{O}$  values for 3 standards measured with a  
361 Picarro analyzer after generation of water vapor using the LHLG.

362

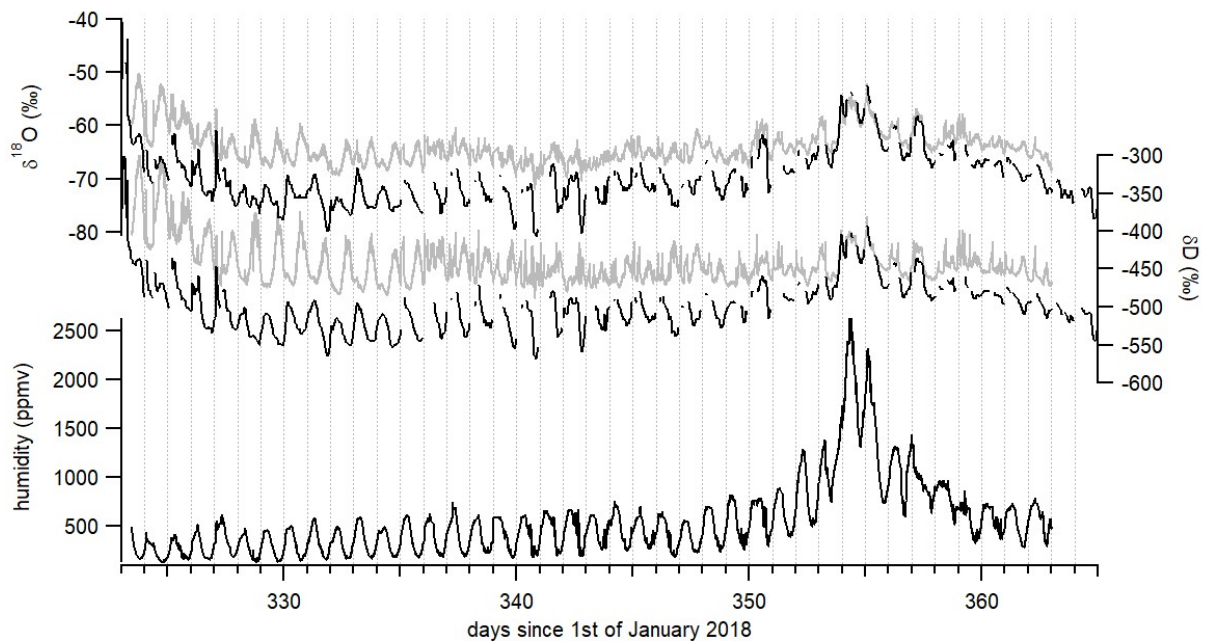
363 We used the measured and true values of EPB and FP5 to estimate the  $\delta^{18}\text{O}$  value of the NEEM standard  
364 from its measured value (Table 3). Using the linear relationship obtained from VSMOW calibrated EPB  
365 and FP5  $\delta^{18}\text{O}$  vs measured EPB and FP5  $\delta^{18}\text{O}$  values following the recommendations of the National  
366 Institute of Standards and Technology (NIST, reference material 8535a) leads to an estimated NEEM  $\delta^{18}\text{O}$   
367 of -33.31 ‰ to be compared to the independently VSMOW calibrated value of -33.5 ‰. Given the  
368 uncertainty of about 0.8-1 ‰ when measuring  $\delta^{18}\text{O}$  around 800 ppmv, we can conclude that the system  
369 is accurate.

370

### 371 **4- Application**

372 The main application of this device is the interpretation of water isotopic profiles at dry sites, in particular  
373 in polar regions. As shown in Figure 5, the influence of humidity on the measurement of the water vapor  
374 isotopic composition with the L2130-i analyzer is large when humidity is below 1,000 ppm and increases  
375 when humidity decreases. Even though the precise isotope ratio-humidity calibration curve is likely to be  
376 different from one analyzer to another, all laser-based water isotope analyzers investigated to date have  
377 shown a strongly non-linear response at low-humidity levels (Guilpart et al., 2017; Leroy Dos-Santos, 2020;

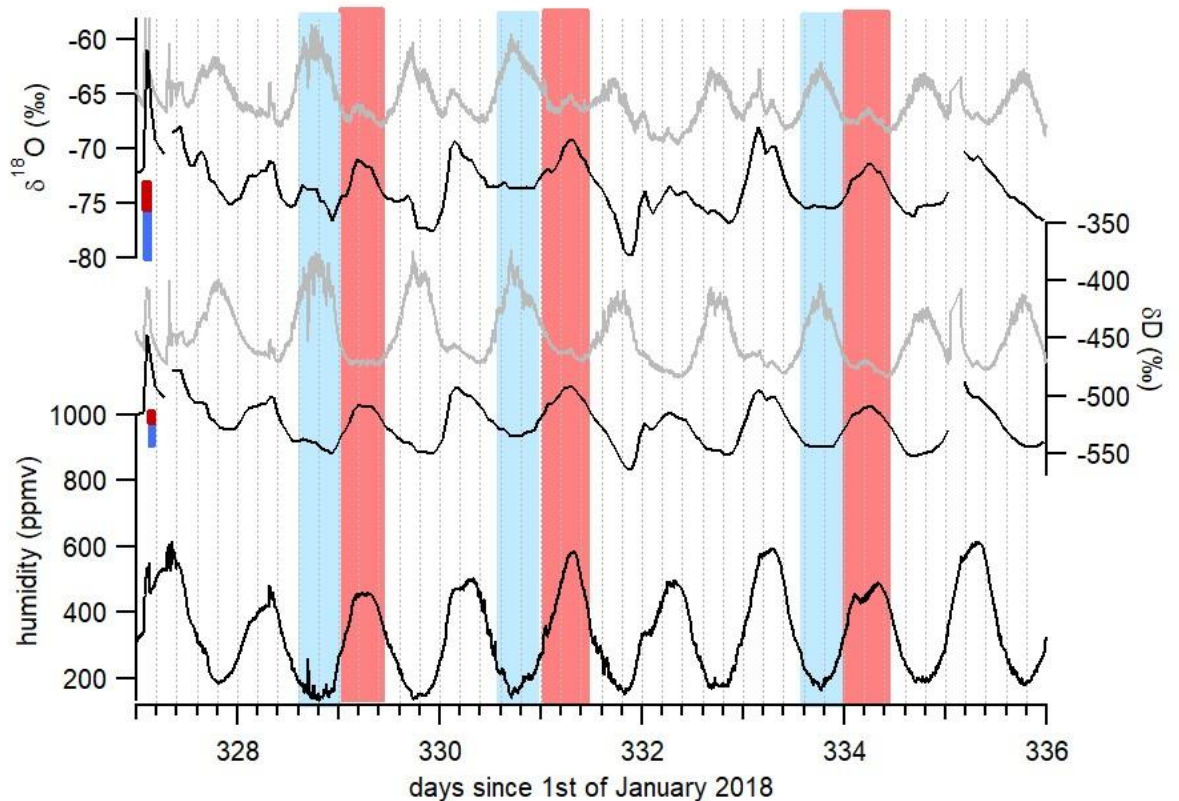
378 Weng et al., 2020). At the Concordia station, even in summer, humidity is generally below 1,000 ppmv  
 379 (Figure 6) so that the interpretation of the diurnal variability of the water vapor isotopic composition is  
 380 strongly affected by the dependency of the measured  $\delta^{18}\text{O}$  and  $\delta\text{D}$  signals on humidity. Figure 6 displays  
 381 such diurnal variabilities during austral summer 2018-2019 at Concordia and the consequently large  
 382 correction of the isotopic records (uncorrected in grey and corrected in black).



383  
 384 **Figure 6:**  $\delta^{18}\text{O}$ ,  $\delta\text{D}$  and humidity records over December 2018 and beginning of January 2019. Raw isotopic  
 385 values are in grey. Corrected isotopic values at hourly resolution are in black after correction of the  
 386 influence of humidity on the water isotopic ratios and adjustment of  $\delta^{18}\text{O}$  and  $\delta\text{D}$  values on the VSMOW-  
 387 VSLAP scale using relationships between measured lab-standard values and known VSMOW calibrated lab-  
 388 standard values.

389  
 390 The data clearly demonstrate the importance of the humidity correction which shifts the curves generally  
 391 to lower isotopic ratio values. However, the difference between uncorrected and corrected data is  
 392 particularly important in the observation of the diurnal variability, illustrated even better when zooming  
 393 in on a section of the data, as in Figure 7. When looking in detail at the diurnal variability in the raw  $\delta^{18}\text{O}$   
 394 and  $\delta\text{D}$  isotope data, some periods stand out with two identified daily peaks, one in phase with the  
 395 humidity peak (marked in red in Figure 7) and one occurring during the period of minimum humidity  
 396 (marked in blue in Figure 7). The strong non-linearity of the calibration curve of Figure 5 suggests that  
 397 artificial peaks in  $\delta^{18}\text{O}$  and  $\delta\text{D}$  could be due to changing humidity levels. Indeed, after correcting the data  
 398 for the humidity dependence of the analyzer (black curve in Figure 7), the isotopic peaks occurring during  
 399 humidity minima are diminished or disappear altogether, while the peaks occurring during humidity  
 400 maxima are amplified. More strikingly, the phase of the signal changes by practically 180° over some

401 periods. Whereas the raw isotope signal peaks during the night, the corrected record shows higher isotope  
 402 ratios during daytime. The diurnal variability recorded on both raw and corrected isotopic values during a  
 403 period with higher humidity level, hence when the isotope ratio-humidity correction is smaller (around  
 404 day 355 in figure 6), also shows that the  $\delta^{18}\text{O}$  ( $\delta\text{D}$ ) diurnal cycles are indeed in-phase with the humidity  
 405 cycle. This result confirms the correlation between humidity cycles and  $\delta^{18}\text{O}$  and  $\delta\text{D}$  of the water vapor at  
 406 the daily scale at Concordia as reported by Casado et al. (2016). We thus conclude that the anticorrelation  
 407 observed between  $\delta^{18}\text{O}$  ( $\delta\text{D}$ ) and humidity in the raw data (highlighted in blue in Figure 7) during periods  
 408 of low-humidity is an artefact due to the influence of the humidity level on the vapor isotopic  
 409 measurements by the L2130-i analyzer.



410  
 411 **Figure 7:** Focus on diurnal variability of  $\delta^{18}\text{O}$ ,  $\delta\text{D}$  and humidity recorded at Concordia. Grey curves show the  
 412 raw measurements and black curves the corrected records. The red (blue) bars indicate the calculated  
 413 uncertainty due to the isotopic ratio vs humidity dependence (Figure 5) on the corrected  $\delta^{18}\text{O}$  and  $\delta\text{D}$  values  
 414 during periods with maximum (minimum) humidity. The red (blue) rectangles indicate half day with  
 415 maximum (minimum) humidity.

416  
 417 **5- Conclusion**  
 418 We have developed an autonomous instrument for low-humidity generation (70 to 2,400 ppmv) with  
 419 controlled water vapor isotopic composition specifically aimed at carrying out continuous measurements  
 420 of the water vapor isotopic composition using a laser-based spectrometer in regions characterized by very

421 low-humidity, such as polar regions. If needed, an interface permits to conveniently connect the new LHLG  
422 to the valve sequencer port of commercial Picarro instruments. After more than one year of routine  
423 operation on two Antarctic sites (Dumont d'Urville and Concordia), this instrument has proven to be very  
424 reliable and robust. It consistently generates stable humidity levels with a  $1\sigma$  variability lower than 10  
425 ppmv over more than 10 minutes. Besides, its performance is significantly better than that of the Picarro  
426 SDM at low humidity.

427 We used this instrument for the calibration of our water isotopic data with a special focus on accurately  
428 quantifying the influence of humidity on the measured isotopic composition of the water vapor. This effect  
429 is huge at low-humidity. We showed that this has an important impact on the interpretation of the diurnal  
430 cycles of  $\delta^{18}\text{O}$  and  $\delta\text{D}$  in the water vapor at the Concordia station at humidity below 1,500 ppmv. We were  
431 able to confirm that, at this site, the diurnal  $\delta^{18}\text{O}$  and  $\delta\text{D}$  variability is actually correlated with humidity  
432 variability, which would not have been possible without the new LHLG instrument.

433 Finally, the development of such an instrument is an important step forward to a better understanding of  
434 the transfer function between climate parameters and the isotopic composition of deep ice cores from  
435 the remote East Antarctic plateau, especially in the context of the new program "Beyond EPICA". It should  
436 be completed by ongoing development of laser spectrometers better adapted to low-humidity levels, such  
437 as those based on the technique of Optical Feedback Cavity Enhanced Absorption Spectroscopy (OFCEAS)  
438 (Casado et al., 2016; Landsberg, 2014; Landsberg et al., 2014).

439

#### 440 **Code availability**

441 The software (HumGen) can be downloaded on line (<https://github.com/ojsd/humgen>;  
442 <https://doi.org/10.5281/zenodo.4003465>).

443

#### 444 **Competing interests**

445 The authors declare that they do not have any competing interest.

446

#### 447 **Author contributions**

448 CLDS, MC, FP and EK designed and built the instrument. OJ realized the software interface development.  
449 CLDS, MC and AL installed the instrument in Antarctica and tested it extensively. EK, SK, MF, AL and EF  
450 tested the instrument in the laboratory. AL wrote the manuscript with the help of all co-authors.

451

#### 452 **Acknowledgments**

453 The development presented in this manuscript is largely inspired from the initial PhD work of Janek  
454 Landsberg which we gratefully acknowledge here. The research leading to these results has received  
455 funding from the Antarctic Snow program of the Fondation Prince Albert II de Monaco, the ANR EAIIST and



456 CNRS-LEFE program ADELISE. The deployment of this instrument in the field was made possible through  
457 the logistic support of the NIVO2 & ADELISE IPEV programs. We thank the two reviewers for their useful  
458 comments which greatly improved the manuscript.

459

## 460 **References**

461 Aemisegger, F., Sturm, P., Graf, P., Sodemann, H., Pfahl, S., Knohl, A. and Wernli, H.: Measuring variations  
462  $\delta^{18}\text{O}$  and  $\delta^2\text{H}$  in atmospheric water vapour using two commercial laser-based spectrometers: an  
463 instrument characterisation study, *Atmos. Meas. Tech.*, 5(7), 1491–1511, doi:10.5194/amt-5-1491-2012,  
464 2012.

465 Bailey, H. L., Kaufman, D. S., Henderson, A. C. G. and Leng, M. J.: Synoptic scale controls on the  $\delta^{18}\text{O}$  in  
466 precipitation across Beringia, *Geophys. Res. Lett.*, 42(11), 4608–4616, doi:10.1002/2015GL063983, 2015.

467 Bastrikov, V., Steen-Larsen, H. C., Masson-Delmotte, V., Griбанov, K., Cattani, O., Jouzel, J. and Zakharov,  
468 V.: Continuous measurements of atmospheric water vapour isotopes in western Siberia (Kourovka),  
469 *Atmos. Meas. Tech.*, 7(6), 1763–1776, doi:10.5194/amt-7-1763-2014, 2014.

470 Bonne, J.-L., Masson-Delmotte, V., Cattani, O., Delmotte, M., Risi, C., Sodemann, H. and Steen-Larsen, H.  
471 C.: The isotopic composition of water vapour and precipitation in Ivittuut, southern Greenland, *Atmos.*  
472 *Chem. Phys.*, 14(9), 4419–4439, doi:10.5194/acp-14-4419-2014, 2014.

473 Bréant, C., Leroy Dos Santos, C., Agosta, C., Casado, M., Fourré, E., Goursaud, S., Masson-Delmotte, V.,  
474 Favier, V., Cattani, O., Prié, F., Golly, B., Orsi, A., Martinerie, P. and Landais, A.: Coastal water vapor isotopic  
475 composition driven by katabatic wind variability in summer at Dumont d’Urville, coastal East Antarctica,  
476 *Earth Planet. Sci. Lett.*, 514, 37–47, doi:10.1016/j.epsl.2019.03.004, 2019.

477 Casado, M., Landais, A., Masson-Delmotte, V., Genthon, C., Kerstel, E., Kassi, S., Arnaud, L., Picard, G., Prie,  
478 F., Cattani, O., Steen-Larsen, H.-C., Vignon, E. and Cermak, P.: Continuous measurements of isotopic  
479 composition of water vapour on the East Antarctic Plateau, *Atmos. Chem. Phys. Discuss.*, 1–26,  
480 doi:10.5194/acp-2016-8, 2016.

481 Casado, M., Landais, A., Picard, G., Münch, T., Laepple, T., Stenni, B., Dreossi, G., Ekaykin, A., Arnaud, L.,  
482 Genthon, C., Touzeau, A., Masson-Delmotte, V. and Jouzel, J.: Archival processes of the water stable  
483 isotope signal in East Antarctic ice cores, *Cryosphere*, 12(5), doi:10.5194/tc-12-1745-2018, 2018.

484 Dong, F. and Baer, D. Development and Deployment of a Portable Water Isotope Analyzer for Accurate,  
485 Continuous and High-Frequency Oxygen and Hydrogen Isotope Measurements in Water Vapor and Liquid  
486 Water, in *Geophysical Research Abstracts*, 12:EGU2010-5571, 2010.

487 Ellehoj, M. D., Steen-Larsen, H. C., Johnsen, S. J. and Madsen, M. B.: Ice-vapor equilibrium fractionation  
488 factor of hydrogen and oxygen isotopes: Experimental investigations and implications for stable water  
489 isotope studies, *Rapid Commun. Mass Spectrom.*, 27(19), 2149–2158, doi:10.1002/rcm.6668, 2013.

490 Genthon, C., Piard, L., Vignon, E., Madeleine, J.-B., Casado, M. and Gallée, H.: Atmospheric moisture  
491 supersaturation in the near-surface atmosphere at Dome C, Antarctic Plateau, *Atmos. Chem. Phys.*, 17(1),  
492 691–704, doi:10.5194/acp-17-691-2017, 2017.

493 Gkinis, V., Popp, T. J., Johnsen, S. J. and Blunier, T.: A continuous stream flash evaporator for the calibration  
494 of an IR cavity ring-down spectrometer for the isotopic analysis of water, *Isotopes Environ. Health Stud.*,  
495 46(4), 463–475, doi:10.1080/10256016.2010.538052, 2010.

496 Guilpart, E., Vimeux, F., Evan, S., Brioude, J., Metzger, J., Barthe, C., Risi, C. and Cattani, O.: The isotopic  
497 composition of near-surface water vapor at the Maïdo observatory (Reunion Island, southwestern Indian  
498 Ocean) documents the controls of the humidity of the subtropical troposphere, *J. Geophys. Res. Atmos.*,  
499 122(18), 9628–9650, doi:10.1002/2017JD026791, 2017.

500 Iannone, R., Romanini, D., Kassi, S., Meijer, H. A. J. and Kerstel, E.: A Microdrop Generator for the  
501 Calibration of a Water Vapor Isotope Ratio Spectrometer, *J. Atmos. Ocean. Technol.*, 26,  
502 doi:10.1175/2008JTECHA1218.1, 2009.

503 Jouzel, J., Masson-Delmotte, V., Cattani, O., Dreyfus, G., Falourd, S., Hoffmann, G., Minster, B., Nouet, J.,  
504 Barnola, J. M., Chappellaz, J., Fischer, H., Gallet, J. C., Johnsen, S., Leuenberger, M., Loulergue, L., Luethi,  
505 D., Oerter, H., Parrenin, F., Raisbeck, G., Raynaud, D., Schilt, a, Schwander, J., Selmo, E., Souchez, R.,  
506 Spahni, R., Stauffer, B., Steffensen, J. P., Stenni, B., Stocker, T. F., Tison, J. L., Werner, M. and Wolff, E. W.:  
507 Orbital and millennial Antarctic climate variability over the past 800,000 years., *Science*, 317(5839), 793–  
508 796, doi:10.1126/science.1141038, 2007.

509 Kerstel, E. Modeling the Dynamic Behavior of a Droplet Evaporation Device for the Delivery of Isotopically  
510 Calibrated Low-Humidity Water Vapor, *Atmospheric Measurement Techniques Discussions*, 1–19.  
511 <https://doi.org/10.5194/amt-2020-428>, 2020.

512 Kopec, B., Lauder, A., Posmentier, E. and Feng, X.: The diel cycle of water vapor in west Greenland, *J.*  
513 *Geophys. Res. Atmos.*, 119(15), 9386–9399, 2014.

514 Landsberg, J.: Développement d'un spectromètre laser OF-CEAS pour les mesures des isotopes de la  
515 vapeur d'eau aux concentrations de l'eau basses. [online] Available from:  
516 <http://www.theses.fr/2014GRENY052/document>, 2014.

517 Landsberg, J., Romanini, D. and Kerstel, E.: Very high finesse optical-feedback cavity-enhanced absorption  
518 spectrometer for low concentration water vapor isotope analyses., *Opt. Lett.*, 39(7), 1795–1798,  
519 doi:10.1364/OL.39.001795, 2014.

520 Lee, X., Sargent, S., Smith, R. and Tanner, B.: In Situ Measurement of the Water Vapor  $^{18}\text{O}/^{16}\text{O}$  Isotope  
521 Ratio for Atmospheric and Ecological Applications, *J. Atmos. Ocean. Technol.*, 22(5), 555–565,  
522 doi:10.1175/JTECH1719.1, 2005.

523 Leroy Dos Santos, C., Masson-Delmotte, V., Casado, M., Fourré, E., Steen-Larsen, H-C, Maturilli, M., Orsi,  
524 A., Berchet, A., Cattani, O., Minster, B., Gherardi, J. and Landais, A., A 4.5 year-long record of Svalbard  
525 water vapor isotopic composition documents winter air mass origin, *J. Geophys. Research*, 125 (23),  
526 (10.1029/2020JD032681), 2020.

527 Ritter, F., Steen-larsen, H. C., Werner, M., Masson-Delmotte, V., Orsi, A., Behrens, M., Birnbaum, G.,  
528 Freitag, J., Risi, C. and Kipfstuhl, S.: Isotopic exchange on the diurnal scale between near-surface snow and  
529 lower atmospheric water vapor at Kohnen station , East Antarctica, *J. Geophys. Research (February)*, 1–  
530 35, doi:10.5194/tc-2016-4, 2016.

531 Sayres, David S, E J Moyer, T F Hanisco, J M St Clair, F N Keutsch, A O'Brien, N T Allen, et al., A New Cavity  
532 Based Absorption Instrument for Detection of Water Isotopologues in the Upper Troposphere and Lower  
533 Stratosphere. *Review of Scientific Instruments* 80 (4): 44102–14.  
534 <http://link.aip.org/link/?RSI/80/044102/1>, 2009.

535 Schmidt, M., Maseyk, K., Lett, C., Biron, P., Richard, P., Bariac, T. and Seibt, U.: Concentration effects on  
536 laser-based  $\delta^{18}\text{O}$  and  $\delta^2\text{H}$  measurements and implications for the calibration of vapour measurements with  
537 liquid standards, *Rapid Commun. Mass Spectrom.*, 24(24), 3553–3561, doi:10.1002/rcm.4813, 2010.

538 Sodemann, H., Aemisegger, F., Pfahl, S., Bitter, M., Corsmeier, U., Feuerle, T., Graf, P., Hankers, R., Hsiao,  
539 G., Schulz, H., Wieser, A. and Wernli, H.: The stable isotopic composition of water vapour above Corsica  
540 during the HyMeX SOP1 campaign: Insight into vertical mixing processes from lower-tropospheric survey  
541 flights, *Atmos. Chem. Phys.*, 17(9), 6125–6151, doi:10.5194/acp-17-6125-2017, 2017.

542 Steen-Larsen, H. C., Masson-Delmotte, V., Hirabayashi, M., Winkler, R., Satow, K., Prié, F., Bayou, N., Brun,  
543 E., Cuffey, K. M., Dahl-Jensen, D., Dumont, M., Guillevic, M., Kipfstuhl, S., Landais, A., Popp, T., Risi, C.,  
544 Steffen, K., Stenni, B. and Sveinbjörnsdóttir, A. E.: What controls the isotopic composition of Greenland  
545 surface snow?, *Clim. Past*, 10(1), 377–392, doi:10.5194/cp-10-377-2014, 2014.

546 Sturm, P. and Knohl, A.: Water vapor  $\delta^2\text{H}$  and  $\delta^{18}\text{O}$  measurements using off-axis integrated cavity output  
547 spectroscopy, *Atmos. Meas. Tech. Discuss.*, 2(4), 2055–2085, doi:10.5194/amtd-2-2055-2009, 2009.

548 Tremoy, G., Vimeux, F., Cattani, O., Mayaki, S., Souley, I. and Favreau, G.: Measurements of water vapor  
549 isotope ratios with wavelength-scanned cavity ring-down spectroscopy technology: new insights and  
550 important caveats for deuterium excess measurements in tropical areas in comparison with isotope-ratio  
551 mass spectrometry, *Rapid Commun. Mass Spectrom.*, 25(23), 3469–3480, doi:10.1002/rcm.5252, 2011.

552 Wang, L., Caylor, K. and Dragoni, D.: On the calibration of continuous, high-precision  $\delta^{18}\text{O}$  and  $\delta^2\text{H}$   
553 measurements using an off-axis integrated cavity output spectrometer, *Rapid Commun. Mass Spectrom.*,  
554 23, 530–536, doi:10.1002/rcm.3905, 2009.

555 Weng, Y., Touzeau, A. and Sodemann, H.: Impact of isotope composition on the humidity dependency  
556 correction of water vapour isotope measurements with infra-red cavity ring-down spectrometers, *Atmos.*  
557 *Meas. Tech.*, 13, 3167–3190, <https://doi.org/10.5194/amt-13-3167-2020>, 2020.

558

559

560

561